RESEARCH ARTICLE

Grid Forming Inverter Power Control Stability Analysis

JUNSU PARK[1], (Student Member, IEEE), SOSEUL JEONG[2], (Member, IEEE), AND MINHAN YOON[1], (Member, IEEE)

[1]Department of Electrical Engineering, Kwangwoon University, Seoul 01897, South Korea
[2]Distributed Power System Research Center, Korea Electrotechnology Research Institute, Gwangju 61751, South Korea

Corresponding author: Minhan Yoon (minhan.yoon@gmail.com)

ABSTRACT Stable system operation is being actively attempted by introducing grid-forming inverters (GFMs) which mimic synchronous generators (SGs). Although the introduction of GFMs intended to replace traditional grid-following inverters (GFLs) provides system inertia and contributes significantly to fault current, it paradoxically exhibits unstable output characteristics under high short circuit ratio (SCR) conditions. In this paper, a mathematical plant model of the basic GFM structure is implemented along with the model integrating grid-connected GFM and the SCR of the system for maintaining the grid dynamics. For this end, a single input single output (SISO) model of an GFM with active power control (APC) is proposed for analyzing the stability in small grid events, and the system frequency response model considering the dynamic performance of SG and GFM APC was also configured for simulating large grid events. The performance of the proposed APC for step response and frequency response characteristics is compared with an existing APC method, such as droop and virtual synchronous machine (VSM). Simulation results using MATLAB and PSS/e verify the performance of the proposed method and stable operation can be expected by actively composing the controller during the SCR that continuously changes in both small and large grid events.

INDEX TERMS Grid-forming inverter (GFM), active power control (APC), single input single output (SISO) modeling, Nyquist stability, short circuit ratio (SCR), droop, virtual synchronous machine (VSM), system frequency response (SFR).

I. INTRODUCTION

The trend of transforming the supply structure of renewable energy is gradually increasing. Renewable energy sources based on power electronic equipment are rapidly replacing existing synchronous generators (SGs). Renewable energy sources, including wind turbine, solar photovoltaics (PV), and energy storage system (ESS), are also called inverter-based resources (IBRs), and these resources are already being used in our daily lives to cover a considerable proportion of electricity demand.

The associate editor coordinating the review of this manuscript and approving it for publication was Meng Huang.

Currently, IBRs connected to the power system simply injects power into the system by following the magnitude, phase angle, and frequency of the voltage at the point of common coupling (PCC). Most IBRs have the control structure called grid-following inverters (GFLs). As the integration of GFL-based IBR resources expands, the following problems have been encountered. The lack of grid transient stability contributes to fault currents and stability problems in the phase-locked loop (PLL) dynamics at low short circuit ratio (SCR) has been addressed [1], [2]. The inertia of the system decreases owing to the physical inertial energy limitation, and the stability of the frequency decreases accordingly. In this context, the grid-forming inverter (GFM) has been attracting attention as a technique that can contribute to the increase

of the system transient stability and inertial resources [3], [4]. Unlike the GFL that operates as a current source, GFM controls the voltage and phase angle itself and operates as a voltage source that imitates the SG.

Since the recent introduction of GFM, it has been widely integrated into system operation, and various GFM control methods have been proposed for increasing system robustness. Droop control has been applied as a basic scheme to develop the most fundamental linear control system [5], [6]. It contains the SG characteristics of $P - f$ and $Q - V$ for frequency and voltage regulation. Research on power loops has been conducted in virtual synchronous machine (VSM) cases, wherein the swing equation of GFM has been simulated [7], [8]. Matching control reflects the dynamic response of a capacitor. It is similar to the swing equation of an SG and generates a phase angle by considering the DC current [9]. Departing from previous machine-based controllers, virtual oscillator control (VOC) is a nonlinear oscillator that comprises dead zone and Van der Pol oscillators [10], [11]. In these various GFM control schemes called active power control (APC), several results have been presented, where GFM control through various controller configurations present an advantage in the dynamic performance of the system in disturbance scenarios or fault current contributions. However, high SCR conditions can pose challenges to GFM, potentially leading to instability in voltage and frequency regulation [12], [13]. Advanced control strategies are therefore essential to stabilize grid forming capabilities under such conditions. Regarding the relationship between SCR of a system and GFM, studies have shown that as SCR increases, the self-synchronization of GFM becomes increasingly unstable [14], [15]. As the SCR increases, even a slight phase difference between the GFM and the system generates large active power variations [16]. An analysis of the frequency response characteristics considering various GFM APC control was presented in the context of a load increase, and a problem that could diverge in specific control conditions, such as parameter setting, was identified [17], [18].

Plant model research based on mathematical models has been conducted to analyze the stability of IBR resources, which may be unstable for systems in small grid events. The single-input-single-output (SISO) transfer function was established based on an LC filter [19], [20]. A damping resistor was added to the capacitor to solve the resonance that occurs from the use of an inverter filter [21], [22]. As the filter-configured GFM operates as a voltage source, it is necessary to analyze the plant model that operates as a voltage source. Additionally, the correlation between the impedance and control-loop gain was investigated by constructing a plant model [23]. A framework for stability analysis was presented by proposing a relational expression between the voltage-controlled plant model and the system SCR through the inverter equivalent impedance [24]. Finally, it is necessary to analyze the stability of the active power by combining the GFM plant model and the APC, which involves the

actual active power output of the GFM. Efforts to integrate APC and plant model for SISO have been made as follows. A small-signal model was analyzed by decoupling the active and reactive powers [25], [26] and a parametric design was presented using a decoupling analysis model [27]. The stability of the active power angle between grid-connected inverters was studied [28]. The transfer function of the GFM APC was obtained, and a stability analysis for the phase margin was conducted [18]. A second-order voltage transfer function was configured with the APC using a voltage plant model as an approximate [29]. A robust parametric tuning design for droop and VSM that could set a stability margin, regardless of the SCR, was presented [30]. A sensitivity analysis was conducted based on the APC parameters in conjunction with SCR [31].

Even if the APC controller is configured by setting in a stable area range considering SCR and stability in small grid events, the GFM configured with the same controller parameters could diverge in large grid events [16], [17]. As stability analysis of large grid events is used for a system frequency response (SFR) [32], not the SISO model of active power, other methods to maintain stable active power of GFM in large grid events must be studied. However, research that configures a stable controller setting in an adaptive method for both small and large grid events and an accurate mathematical frequency analysis model for GFM APC and SG dynamics is lacking.

Therefore, this study makes the following contributions:

1) Stability analysis based on the SCR was conducted using the simplified active power SISO model with plant model and APC.

2) APC was set adaptively using the proposed method considering SCR and the stability was improved in both Nyquist stability criterion and step response.

3) An accurate mathematical-based SFR model considering the proposed method of a GFM APC was presented and proven to be stable in the time-domain simulation.

4) A proposed GFM APC using an adaptive method for setting parameters improves the transient stability of small and large grid events.

The flow and structure of this paper are as follows: the APC configuration based on the active-power SISO model is described in II. A new controller is presented to solve the stability problem in small-grid events, and the results are presented in III. After a methodology is presented to mathematically interpret the SFR model, the simulation results are compared and verified in IV. Simulation results are obtained using the proposed method for large-grid events in V. Finally, the conclusions are presented in VI.

II. GFM INVERTER MODELING
A. VOLTAGE-CONTROLLED PLANT MODEL
Fig. 1 shows the basic control structure of the voltage-source-based GFM inverter. It contains a cascaded structure in which a current reference value is generated using the voltage control loop and a voltage reference value for pulse width
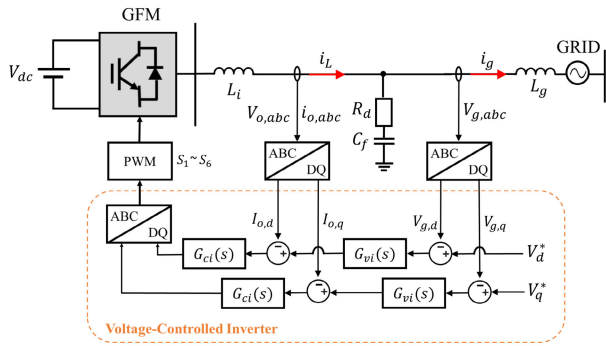
FIGURE 1. Structure of the voltage-controlled inverter control circuit.

modulation (PWM) switching is generated in the current control loop. In this study, an LC-filter-based voltage source model is analyzed, and GFM was connected to the grid via the system impedance $Z_{lv} = \omega L_g s + R_g$. Herein, L_g based on per unit (p.u.) can be expressed as SCR, and SCR = $1/Z_{lv}$. Accordingly, SCR becomes a criterion for checking the robustness of PCC when the GFM is connected to the grid.

The voltage-source-based control structure of the GFM inverter shown in Fig. 1 can be implemented as a control block diagram for the system shown in Fig. 2. Using the superposition principle, $G_{clv}(s)$ and the equivalent impedance of the inverter $Z_{ov}(s)$ are composed. The derivation process for each transfer function is expressed in Eq. (1)∼(7). $G_{clv}(s)$ receives the voltage reference $V_o^*(s)$ and generates voltage. $Z_{ov}(s)$ is combined with the grid current $i_g(s)$ to form the transfer function for the $V_o(s)$ as the disturbance part [24].

$$V_o(s) = G_{clv}(s)V_o^*(s) - Z_{ov}(s)i_g(s) \tag{1}$$

$$Y_{Li}(s) = \frac{1}{Z_{Lf}(s) + Z_{Cf}(s)} \tag{2}$$

$$G_{ii}(s) = \frac{Z_{Cf}(s)}{Z_{Lf}(s) + Z_{Cf}(s)} \tag{3}$$

$$G_{clv}(s) = \frac{T_v(s)}{1 + T_v(s)}, \quad Z_{ov}(s) = \frac{Z_{oi}(s)}{1 + T_v(s)} \tag{4}$$

$$T_v(s) = \frac{G_{vi}(s)G_{ci}(s)G_{PWM}(s)Z_{Cf}(s)}{Z_{Lf}(s) + Z_{Cf}(s) + G_{ci}(s) * G_{PWM}(s)} \tag{5}$$

$$Z_{oi}(s) = \frac{Z_{Cf}(s)[Z_{Lf}(s) + G_{ci}(s) * G_{PWM}(s)]}{Z_{Lf}(s) + Z_{Cf}(s) + G_{ci}(s) * G_{PWM}(s)} \tag{6}$$

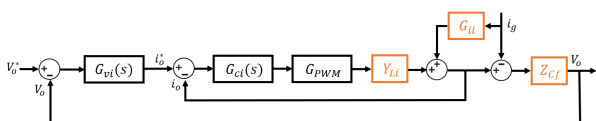$$G_{vi}(s) = K_{vp} + \frac{K_{vi}}{s} \tag{7}$$

FIGURE 2. Block diagram of the voltage-controlled inverter.

$Z_{Lf}(s)$ and $Z_{Cf}(s)$ represent the impedance of the filter inductor and a capacitor with a damping resistor.
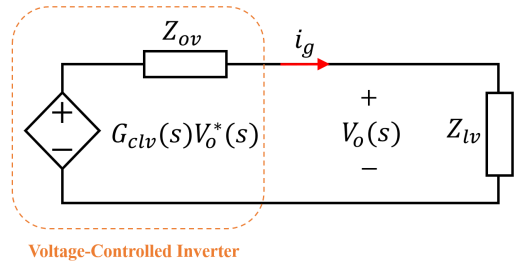

Voltage-Controlled Inverter

FIGURE 3. Impedance-based equivalent model for voltage-controlled inverter.

$G_{vi}(s)$ indicates the proportional-integral (PI) controller of the voltage control loop. $G_{ci}(s)$ is the proportional (P) current controller. Since PWM has a sufficiently high switching frequency and almost no time delay, this is assumed to be $G_{PWM}(s) \approx 1$. In summary, the plant model was interpreted as a transfer function for the voltage in Eq. (1). It is described as an impedance-based equivalent model of Eq. (1) and shown in Fig. 3.

As shown in Fig. 3, GFM operating as a voltage source is controlled by $G_{clv}(s)$. The equivalent impedance $Z_{ov}(s)$ of the inverter and impedance $Z_{lv}(s) = \omega L_g s + R_g$ of the grid are connected in series. $Z_{lv}(s)$ can be regarded as the SCR of the GFM-connected bus, and $V_o(s)$ applied based on the voltage reference $V_o^*(s)$ can be constructed using the equivalent impedance of the inverter and system SCR, as expressed in Eq. (8). It is the closed-loop transfer function of the GFM plant model considering the GFM voltage control part and the SCR of the system [24].

$$\frac{V_o}{V_o^*(s)} = G_{clv}(s)\frac{1}{1 + \frac{Z_{ov}(s)}{Z_{lv}(s)}} = G_v(s) \tag{8}$$

B. GFM PLANT MODEL POLE CONSIDERING THE SCR

Table 1 lists the parameters applied to the voltage-source-based GFM. The plant model $G_v(s)$ was analyzed based on the SCR. The plant model for Eq. (8) was implemented in MATLAB based on a transfer function without a PI controller $G_{vi}(s)$. Since the equation changes based on the SCR, the change pattern of the pole is displayed as the SCR changes.

Fig. 4 illustrates that the pole of $G_v(s)$ moves to the right half as the SCR increases. Based on the currently set LC filter value, the corresponding $G_v(s)$ pole has a real axis value of $-42\sim-40$, which indicates a stable condition. However, this is simply a characteristic of the plant model regarding GFM voltage, and it is necessary to analyze the power stability when injecting active power into the system. This is because the grid system is a voltage source and GFM also operates based on a voltage source, so the closer the two voltage sources are, that is, the higher the SCR, the more unstable it is because both of them influence each other with their own ability. Conversely, when two voltage sources are connected far away from each other, that is, when the SCR is low, the system is stable because each voltage source forms a voltage at its location and has little influence on
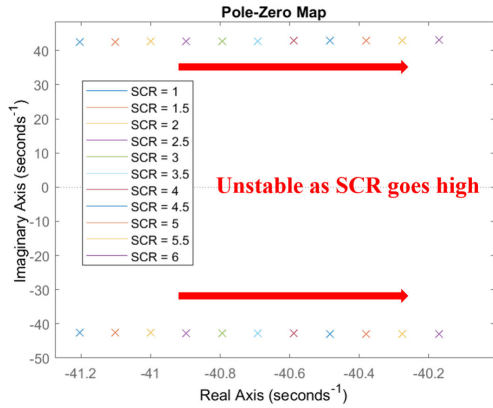
FIGURE 4. Grid-forming (GFM) inverter plant model pole considering the short-circuit ratio (SCR).

each other. The voltage-source-based GFM combined with APC or in conjunction with various system conditions can become unstable as the SCR increases or with the parameter setting of controllers. Therefore, a stability analysis should be conducted by considering the power characteristics of the GFM, including APC, which will be analyzed in the next chapter.

C. POWER LOOP–ACTIVE POWER CONTROL (APC)

Small-signal analysis is required to perform frequency-response-based stability analysis. The analysis is carried out using a small-signal model of the active and reactive power injected into the system of the grid-connected inverter. The active power output comprises an outer control loop added to $G_v(s)$. The outer control loop is composed of an APC that controls the angle and a reactive power control (RPC) that controls the voltage similar to the function of a synchronous generator. In the APC part, a droop control that emulates the droop of the governor and a VSM that can simulate the swing equation and damping of the generator are configured. In the RPC, the voltage reference value is generated based on Q-droop control. However, the focus is on the stability analysis of the active power in the SISO model. Additionally, when robust control parameters are applied, there exists a minor voltage response owing to small changes in the active power; therefore, it is assumed that $V_o^*(s) = V_o(s) = 1$ p.u.

To obtain a GFM power loop based on the SISO model, it is necessary to obtain the small-signal models of active and reactive power parts of the GFM. The outputs of the active and reactive powers are expressed as follows [25]:

$$P = \frac{3V_o[(V_o - V_g \cos \delta_0)R_g + V_g X_g \sin \delta_0]}{2(R_g^2 + X_g^2)} \tag{9}$$

$$Q = \frac{3V_o[(V_o - V_g \cos \delta_0)X_g - V_g R_g \sin \delta_0]}{2(R_g^2 + X_g^2)} \tag{10}$$

δ_0 denotes the phase angle difference between the GFM and the PCC bus of the system when the GFM is grid-connected. $X_g = \omega_0 L_g$, and the small-signal equations

of P and Q for power loop stability analysis are given as follows:

$$\hat{P} = K_{p\delta}\hat{\delta} + K_{pv}\hat{V}_0$$
$$\hat{Q} = K_{q\delta}\hat{\delta} + K_{qv}\hat{V}_0 \tag{11}$$

In general, P is dominant in angle, and Q is dominant in voltage, so only $K_{p\delta}$ and K_{qv} are analyzed in this paper. The expressions for $K_{p\delta}$, K_{qv} are as follows,

$$K_{p\delta} = \frac{3V_o V_g(R_g \sin \delta_0 + X_g \cos \delta_0)}{2(R_g^2 + X_g^2)}$$

$$K_{qv} = \frac{3V_o(2V_o X_g + V_g(-R_g \sin \delta_0 - X_g \cos \delta_0))}{2(R_g^2 + X_g^2)} \tag{12}$$

For a droop-control-based APC, the angular velocity of GFM is as follows,

$$\omega_{oref} = (P_{ref} - P_{meas})\omega_o R_p + \omega_o \tag{13}$$

In the case of RPC based on droop control, the voltage of GFM is as follows,

$$V_{oref} = (Q_{ref} - Q_{meas})V_n R_q + V_n \tag{14}$$

The transfer functions $G_p(s)$ $G_q(s)$ of the APC and RPC controllers are

$$G_p(s) = \frac{\theta_{o,ref}(s)}{P_{ref}(s) - P_{meas}(s)} = \frac{\omega_o R_p}{s}$$

$$G_q(s) = \frac{V_{o,ref}(s)}{Q_{ref}(s) - Q_{meas}(s)} = V_o R_q \tag{15}$$

To simplify the SISO model, it is assumed that only $K_{p\delta}$, which is a relational expression between the active power and δ, is related to the active power measurement P_{meas} of the GFM. As the stability analysis of the active power output equation is conducted, and the voltage is assumed to be 1 p.u, the open-loop transfer function (OLTF) of reactive power is omitted. Referring to Fig. 5, the OLTF of active power is given as follows:

$$G_{p\_open}(s) = G_p(s)G_v(s)K_{p\delta} \tag{16}$$

In $K_{p\delta}$, if $X_g > R_g$ and the initial GFM are synchronized with the system and integrated, a phase angle difference does not exist between the system and the GFM. Therefore, $\delta_0 = 0$. The final simplified OLTF of the active power is equal to Eq. (17).

$$G_{p\_open}(s) = \frac{3}{2X_g}G_p(s)G_v(s) \tag{17}$$

III. PROPOSED CONTROL
A. DIFFERENTIATOR WITH SCR DAMPING (DTSD)
The GFM plant model was found to become unstable based on the SCR. It implies that the active power SISO model may also be unstable if the unstable factor based on the SCR is not properly compensated in the GFM APC. Prior research has demonstrated the need to set droop sensitively and damping to a large setting at high SCR [18]. Therefore, there is a need
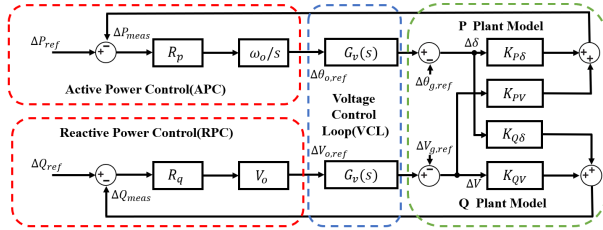
FIGURE 5. APC open-loop transfer function (OLTF).

TABLE 1. Parameters and variable definitions.

Symbol	Name	Value
S_n	Rated capacity	100 MVA
V_g	Rated grid voltage	22.9 kV
ω_o	Fundamental angular frequency	377 rad/s
X_g/R_g	Grid-side impedance X/R ratio	1
L_i	Inverter-side inductance	0.2 mH
C_f	Filter capacitance	20 μF
R_d	Passive damping resistance	0.5 Ω
K_{vi}	Integral gain of voltage controller	25
K_{vp}	Proportional gain of voltage controller	1
K_{cp}	Proportional gain of current controller	1
R_p	Droop control constant	0.05
H_{vsm}	VSM inertia constant	1
D_{vsm}	VSM damping constant	40
T_1	DTSD delay	5.0
α	DTSD alpha	0.8
β	DTSD beta	0.8

to set droop and damping adaptively with reference to SCR. An exponential function form was used to set parameters broadly within various SCR ranges. To prevent the use of arbitrary exponential functions, exponential function with base e was proposed, which suggests appropriate parameter settings in various SCRs. Considering a high SCR can result in unstable characteristics in the existing droop and VSM controls, this study proposes a differentiator with SCR damping (DTSD) controller that considers SCR in the exponential function. The control block diagram of the DTSD can be explained as follows. In the damping part, the SCR is quantified while the GFM is applied to the controller. The GFM can set the droop or damping sensitivity by dynamically controlling α and β based on the SCR. Subsequently, the differentiator component was composed of the droop and VSM with a differentiator time delay T_1, as shown in Fig. 6. DTSD also constitutes the APC of the GFM and can be briefly represented as OLTF as shown in equation (17). While $G_v(s)$ remains the same, $G_p(s)$ of droop including DTSD is as follows.

$$G_p(s) = \frac{\omega_o}{s} \frac{R_p}{(1 + \alpha e^{\beta SCR} R_p)} (1 + \frac{sT_1}{1 + sT_1}) \quad (18)$$

$G_p(s)$ of VSM including DTSD is as follows.

$$G_p(s) = \frac{\omega_o}{s} \frac{1}{2H_{vsm}s + D_{vsm} + \alpha e^{\beta SCR}} (1 + \frac{sT_1}{1 + sT_1}) \quad (19)$$
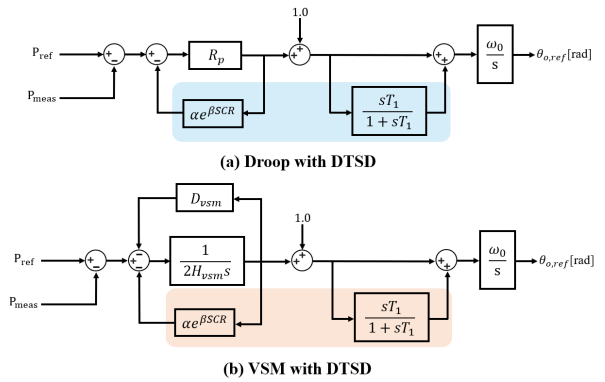

FIGURE 6. Proposed differentiator with SCR damping (DTSD) controller.

The control block, which provides feedback in the droop or inertia part, is a natural exponential function composed of two parameters. GFM can adjust the sensitivity of the overall DTSD controller using α, which is a parameter that controls the degree of influence of the damping. If it is set to a high level, the sensitivity can be increased by further damping the angle. In the case of β, the GFM can adjust the dependence on SCR. The dynamic characteristics of various SCRs can be simulated for large settings. If β is small, the output change can be set to be insignificant by conservatively setting the parameters based on the SCR. Finally, the controller is adaptively configured by setting the SCR as a variable, and the controller is completed by linking the differentiator to form the angle. α, β are set to values between 0 and 1.

B. STABILITY ACCORDING TO DTSD PARAMETERS
Fig. 7 illustrates the Nyquist diagram result of Eq. (17) based on GFM parameters listed in Table 1, and droop with DTSD was used for APC, as shown in Fig. 6. To compare results in terms of α, SCR was set to a high value at 6, and β was fixed at 0.5. As α increases, the damping value based on SCR increases, so droop is set sensitively and moves to the stable area in the Nyquist diagram. When α is 0.2, 0.5, and 0.8. In other words, as the margin is insufficient, additional improvement is required for stable operation.
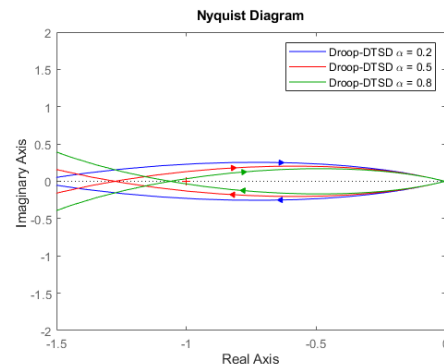

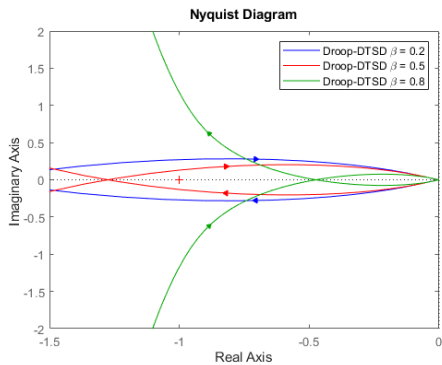**FIGURE 7.** Nyquist plot according to α of Droop-DTSD when SCR = 6 and β=0.5.

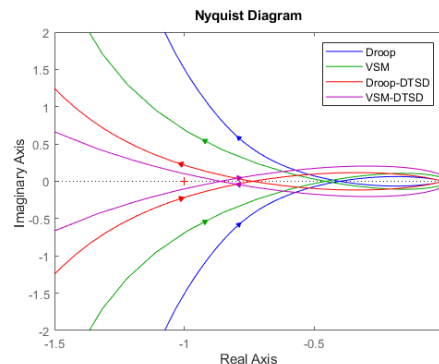**FIGURE 8.** Nyquist plot based on β of Droop-DTSD when SCR = 6 and $\alpha = 0.5$.

FIGURE 9. Nyquist plot of Droop-DTSD for varying SCR when $\alpha = \beta = 0.8$.

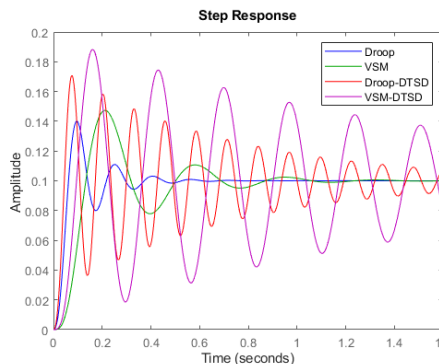**FIGURE 10.** Nyquist plot with the proposed DTSD in low-SCR cases.

FIGURE 11. Step response compared with droop, VSM, and DTSD in low-SCR cases.

Fig. 8 shows the Nyquist diagram based on β when SCR = 6 and $\alpha = 0.5$. In this case, it can be observed that as β increases, stability increases because damping is set more sensitively based on SCR. Importantly, β is a parameter that enters exponential function, so the effect of providing damping is greater when compared to α. Since the damping effect is greater when $\beta = 0.8$ than when $\alpha = 0.8$, as shown in Fig. 7, it appears that a larger stability margin is secured, as shown in Fig. 8. In the case of VSM with DTSD, the Nyquist diagram pattern based on α and β is similar to droop with DTSD; therefore, it was omitted.

Fig. 9 shows the Nyquist plots when alpha and beta are fixed at 0.8 and the SCR values are 1, 3.5, and 6. By setting α and β to a high sensitivity value of 0.8 in droop control with DTSD, it is observed that the Nyquist plots for all SCR conditions do not encircle the point $(-1, 0)$, indicating that the system operates within a stable region. Particularly, at a high SCR value of 6, the system achieves the greatest stability margin, thereby ensuring stable output from the GFM. Consequently, this demonstrates that applying the proposed DTSD technique within the typical SCR range of power systems ensures the stable controller configuration of the GFM.

C. COMPARISON OF VARIOUS POWER LOOP CONTROL SCHEMES WITH NYQUIST IN LOW-SCR CASES

When the SCR was low at 1 with steady-state operation of the droop, VSM, droop with DTSD, and VSM with DTSD were compared. The results show the Nyquist stability analysis of the p.u. based controller $G_{p\_open}(s)$ in Eq. (17) and the step-response results with the parameters listed in Table 1, where both alpha and beta are set to 0.8, are provided. This enables the impact of the power system to be evaluated intuitively by obtaining stability information using the open loop of the controller. Finally, the step response reference value was applied at 0.1 p.u., which is 10% of the GFM rated capacity, and the dynamic performance was compared in MATLAB.

Fig. 10 shows the Nyquist stability analysis results of the GFM active power OLTF proposed in Eq. (17). When the SCR is low, it can be observed that droop, VSM, droop with DTSD, and VSM with DTSD all yield Nyquist diagrams, which are far away from the $(-1, 0)$ point shown in Fig. 10. The observation suggests that the stability area range is generous in the case of a GFM that is connected far away from a grid system with low SCR, and continuous stable output performance can be expected regardless of the type of controller used. When comparing the diagrams, both droop and VSM are within the stable range, but margin of DTSD slightly decreases.

Fig. 11 shows the step response results of APC control in four controllers in MATLAB. Evidently, all of them cause a slight overshoot at the beginning before quickly converging to the reference value. In the cases of VSM, it can be observed that a time delay filter is included and a delay occurs, thus
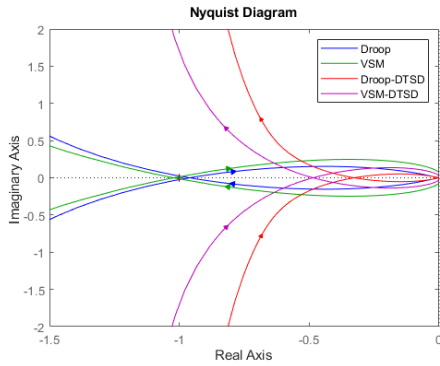
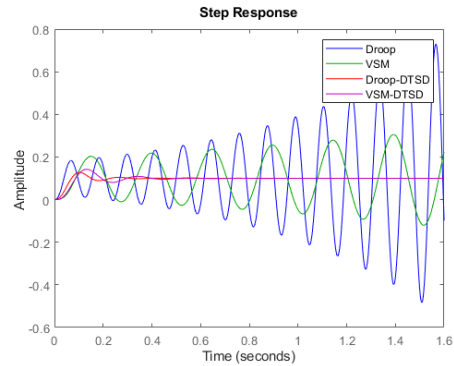**FIGURE 12.** Nyquist plot with the proposed DTSD in high-SCR cases.

FIGURE 13. Step response compared with droop, VSM, and DTSD in high-SCR cases.

converging slowly. In the case of both of DTSD, they converge to the reference with little vibration than without DTSD controllers. Therefore, when SCR is low, all controllers stably converge the reference value in a steady state.

D. COMPARISON OF VARIOUS POWER LOOP CONTROL SCHEMES WITH NYQUIST IN HIGH-SCR CASES

Four controllers were compared when the SCR was 6, which is expected to lead to an unstable steady-state operation of the GFM. The analysis process for stability analysis and step response are the same as those in the previous case for a low SCR, and the same parameters listed in Table 1, with both alpha and beta set to 0.8, were applied to simulate and compare the dynamic response under the same conditions, except SCR.

The Nyquist diagram results shown in Fig. 12 were analyzed as follows in high SCR condition. The results of droop and VSM without DTSD surrounds $(-1, 0)$ show that stability margin is non-existent, which indicates that the power can diverge in any case. In the cases of controllers using DTSD, a margin of stability exists farther than the $(-1, 0)$ point on the Nyquist. This shows that even at high SCR, if the proposed DTSD method is used, more margin will be secured and dynamic performance will be stable in a steady state.

Fig. 13 illustrates the step response result obtained through the stability analysis in Fig. 12. It can be observed that droop and VSM without DTSD diverge the in step response as a stability margin does not exist. On the contrary, droop and VSM using the DTSD method stably converge to the reference value and show stable results in steady state. Accordingly, stability has been increased through the proposed method for operating GFM, which can be unstable at high SCR, and the active power will be maintained by adaptively configuring the controller using SCR when integrated into the power system.

IV. SYSTEM FREQUENCY RESPONSE MODELING

A. SYSTEM FREQUENCY RESPONSE MODELING WITH DROOP, VSM, AND DTSD

Even if APC is constructed by applying stability analysis in small grid events, and improved with proposed method, active

power for frequency response in large grid events should also be analyzed. This is because the frequency responses of GFM are expressed as another mathematical model based on the configuration of the power system such as governor and inertia in large grid events. Additionally, there exists a possibility that the GFM power may diverge based on the APC control parameters of the GFM [17], [18]. Accordingly, this part proceeds with the SFR model and implements it mathematically using the swing equation based on the mechanical characteristics of the SG [32]. Moreover, the process of implementing various APC controls of GFM will be integrated into the SFR model.

In the SFR model, an analysis was conducted using one generator that can simulate the equivalent system and GFM with APC controllers. For the simplified SFR model analysis, the damping factors of the generator and the headroom of the generator were not considered. ΔP_d was applied as a step response for the frequency response. The parameters of the governor are applied with general values from thermal plants [32]. The generator and GFM form frequencies based on the swing equation; therefore, the frequency formation process is given by Eq. (20)∼(22), where s denotes the Laplace derivative term. The frequency formation formula for an SG without considering damping is as follows:

$$\frac{d^2\theta_g}{dt^2} = s\frac{d\theta_g}{dt} = s\omega_g = \frac{\Delta P}{2H}, \Delta\omega_g = \frac{\Delta P}{2Hs} \quad (20)$$

The frequency formation formula for the GFM inverter droop is as follows:

$$\frac{d\theta_o}{dt} = \omega_o = R_p\Delta P \quad (21)$$

The frequency formula for GFM VSM can be expressed as

$$\frac{d\theta_o}{dt} = \omega_o = \frac{1}{2H_{vsm}s + D_{vsm}}\Delta P \quad (22)$$

$\Delta\omega$ is fed back by the governor of the generator to output mechanical power P_m, and the dynamic state of the frequency continuously changes. If the generator and GFM are connected in a synchronized region, $\Delta\omega_g = \Delta\omega_o = \Delta\omega$.
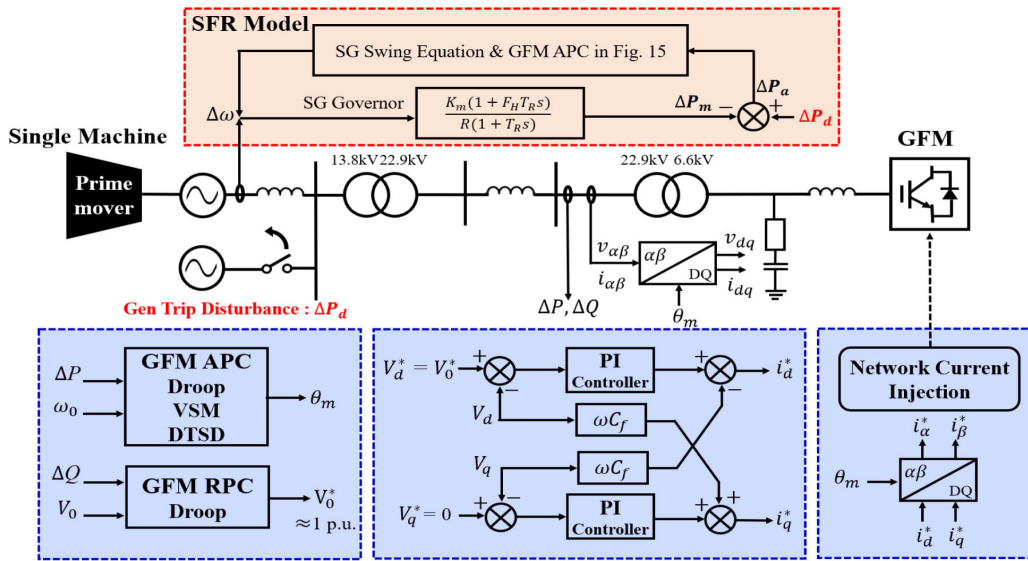
FIGURE 14. Equivalent system structure comprising a generator with governor and GFM.

Therefore, the expressions of $\Delta\omega$ and ΔP_d in SFR that reflect the process thus far are shown in Fig. 15.

The frequency formation formula of droop with DTSD is expressed as

$$\frac{d\theta_o}{dt} = \omega_o = \frac{R_p}{1 + \alpha e^{\beta SCR}R_p}(1 + \frac{sT_1}{1 + sT_1})\Delta P \qquad (23)$$

Subsequently, the frequency formation formula of VSM with DTSD is obtained as

$$\frac{d\theta_o}{dt} = \omega_o = \frac{1}{2H_{vsm}s + D_{vsm} + \alpha e^{\beta SCR}}(1 + \frac{sT_1}{1 + sT_1})\Delta P \qquad (24)$$

B. SFR MODEL VALIDATION

Table 2 summarizes the SG and governor parameters applied to the SFR model. The remaining PI controller gains, filter values, and parameters of DTSD are the same as those listed in Table 1. In the time-domain simulation PSS/e used in this study, a dynamic model that can simulate GFM does not exist. Therefore, a user defined model (UDM) based on numerical integration was modeled for a controller comprising APC, RPC, and voltage control loop with the structure shown in Fig. 14, and this GFM UDM model was integrated into PSS/e system for the simulation of large grid events. To present the improved performance of the proposed method, the results are proved in a test system. As shown in Fig. 14, the test system consists of GFM and SGs with a governor that can equivalently simulate the system, and each power generation source is set to 100 MVA.

In Fig. 16, MATLAB nadir frequency is 59.785 Hz in 1.5 s, Pss/e is 59.7854 Hz in 1.57 s, and both graphs converge to 59.83 Hz for droop. In the case of VSM shown in Fig. 16, the frequency obtained using MATLAB recorded 59.873 Hz
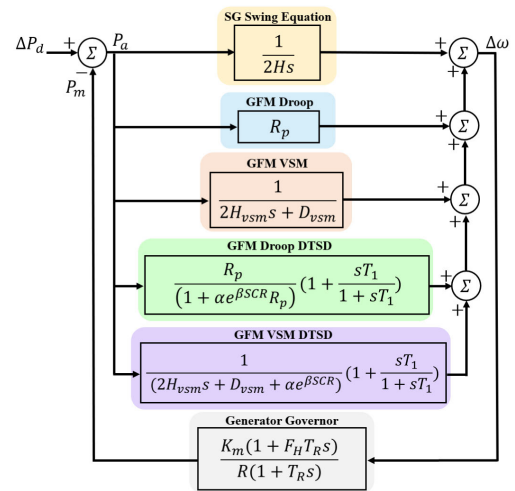

FIGURE 15. System frequency response (SFR) model, including droop, VSM, and DTSD.

TABLE 2. SFR model parameters and simulations.

Symbol	Name	Value
H	Generator inertia	5
R	Governor droop	0.05
K_m	Mechanical power gain factor	1
F_H	Fraction of total power generated by the HP turbine	0.3
T_R	Reheat time constant, s	8.0
ΔP_d	Load step magnitude	0.1

in 1.1 s, PSS/e recorded 59.874Hz in 1.17s, and both converged to 59.89 Hz. In conclusion, based on the MATLAB and PSS/e simulation results, the frequency response is
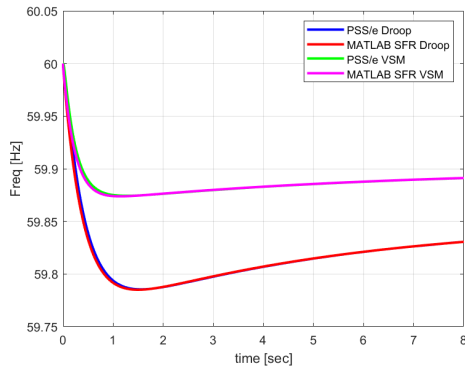
FIGURE 16. Validation of MATLAB SFR model and PSS/e simulation results.

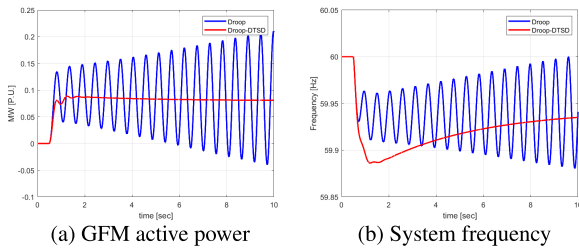(a) GFM active power (b) System frequency

FIGURE 17. Droop and droop with DTSD results in low-droop case.

error-free. Finally, the following two meaningful results can be derived. 1) Several APC controls are proven in the transfer function of GFM. 2) The GFM UDM in PSS/e can be used to analyze the large grid events scenario and frequency response.

V. SIMULATION RESULTS

This section presents the simulation results to compare with the actual divergence cases and compares the performance of the proposed method in a test system, as shown in Fig. 14. The simulation conditions were that SG and GFM were 100 MVA each, and the generator trip was 10 MW, which is 10% of the base capacity. GFM control parameters are based on Table 1, and the SG governor parameters are based on Table 2.

A. UNSTABLE LOW-DROOP CASES

To simulate unstable output situations in droop, droop was set sensitively through SCR damping with α and β based on Table 1, as shown in Fig. 17. Droop was changed from 0.05 to 0.0117 and SCR was assumed to be 6. The sensitive droop value is compared without a differentiator and with differentiator in PSS/e time-domain simulation.

It can be observed that the active power diverges in the case of droop without differentiator, as shown in Fig. 17(a). However, this problem can be solved by injecting a differential DTSD component. In droop with DTSD, droop is also set to be sensitive, and a differentiator is simply integrated into the controller, but the active power is stable. This is because droop combined with differentiator reduces the overshoot and ensures the stability of active power in
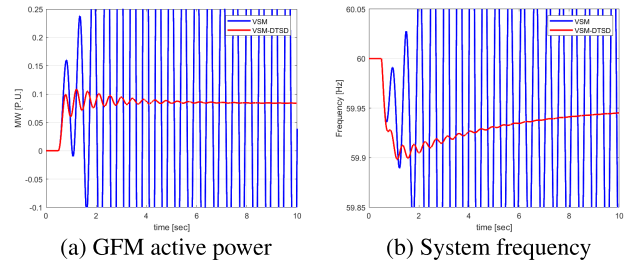

(a) GFM active power (b) System frequency

FIGURE 18. VSM and VSM with DTSD results in the high-damping case.

large grid events. In conclusion, droop with differentiator outputs up to 8.8 MW, which is 0.088 p.u., and converges to 8.1 MW, which is 0.081 p.u. In the case where only droop exists, it appears that overshoot occurs above 10 MW, but it continues to diverge thereafter.

Based on the active power of GFM, the frequency results are shown in Fig. 17(b). In the test system, GFM and SG were set to the same rated capacity as 100 MVA. If GFM injects active power unstable, the overall supply and demand of the active power of the system also becomes unstable. Thus, the output of the GFM has a large influence on the test system. As shown in Fig. 17, when the GFM diverges, the frequency also diverges without stabilizing. However, as the droop with DTSD injects active power stably, the system frequency also changes stably. Droop with differentiator records a nadir frequency of 59.886 Hz and converges to 59.94 Hz, whereas droop without differentiator causes the system frequency to collapse. As shown in the results, performing droop controller design considering the differentiator is essential to avoid power divergence instability of GFM.

B. UNSTABLE VSM CASES WITH HIGH DAMPING

In this subsection, simulation was performed for analyzing the unstable output VSM case. If the damping value of VSM, D_{vsm} is set to a high value and sensitive to active power, the output of the integrator based on the VSM inertia is not properly linked to the voltage control loop parameters, and it could diverge. Therefore, to take an excessive damping value, D_{vsm} is set from 40 to 105.16 based on α and β in Table 1 and SCR was assumed to be 6. The results were compared with and without differentiator in same simulation conditions as droop.

In Fig. 18(a), the damping of VSM is set sensitively; however, if a differentiator is not used, the output diverges. It can be observed that the output of VSM using a differentiator remains stable. As in the previous droop case, the differentiator significantly improves overshoot performance even with sensitive damping value gain. In this case, VSM with differentiator outputs up to 11.0 MW, which is 0.11 p.u., and converges to 8.4 MW, which is 0.084 p.u. In the absence of a differentiator, it initially overshoots beyond 15 MW, and diverges. In the case of VSM, unlike droop, there exists a time delay in the APC owing to the H_{vsm} component, thus greater oscillations may occur. Therefore, if H_{vsm} is set too large,

the time delay becomes larger and more time delay filtering is applied, which may cause the output to become unstable. Therefore, H_{vsm} must be set to an appropriately low value.

If the VSM output is unstable, the system frequency also diverges, as shown in Fig. 18(b). VSM with a differentiator shows a nadir frequency of 59.9 Hz and converges to 59.95 Hz. However, VSM without differentiator also causes the system frequency to collapse. Even in the case of VSM, it can be derived that if the damping value is set to an excessively high value or the damping is increased by the α and β of the proposed DTSD, the output can be maintained stably by utilizing the differentiator.

VI. CONCLUSION

In this study, an SISO model-based, active power OLTF transfer function with APC was established as part of a method that can stabilize by adopting the proposed method, based on the SCR. The performance of the DTSD presented in the small-grid event was proven to be superior to that of the existing droop and VSM based on Nyquist stability analysis and step responses. Additionally, the droop, VSM, and DTSD controllers were mathematically modeled using SFR modeling in large-grid events. By comparing the MATLAB and PSS/e simulation results, this study verified that the transfer function based on various APC was properly configured. Subsequently, a stable output was guaranteed by introducing the proposed DTSD even in sensitive parameter settings of droop and VSM. Therefore, if the proposed method is applied when a GFM is connected to the system, stability problems can be solved in small grid events, while a stable output can be expected in large grid events. For further research, adaptive parameter setting based on the various capacities of GFM should be investigated, and the frequency response should be carried out through detailed SFR, including all IBRs with other frequency control.

REFERENCES

[1] L. Huang, C. Wu, D. Zhou, and F. Blaabjerg, "A double-PLLs-based impedance reshaping method for extending stability range of grid-following inverter under weak grid," *IEEE Trans. Power Electron.*, vol. 37, no. 4, pp. 4091–4104, Apr. 2022.

[2] X. Zhang, D. Xia, Z. Fu, G. Wang, and D. Xu, "An improved feedforward control method considering PLL dynamics to improve weak grid stability of grid-connected inverters," *IEEE Trans. Ind. Appl.*, vol. 54, no. 5, pp. 5143–5151, Sep. 2018.

[3] Q. Hu, R. Han, X. Quan, Z. Wu, C. Tang, W. Li, and W. Wang, "Grid-forming inverter enabled virtual power plants with inertia support capability," *IEEE Trans. Smart Grid*, vol. 13, no. 5, pp. 4134–4143, Sep. 2022.

[4] Y. Lin, J. H. Eto, B. B. Johnson, J. D. Flicker, R. H. Lasseter, H. N. V. Pico, G.-S. Seo, B. J. Pierre, and A. Ellis, "Research roadmap on grid forming inverters," Nat. Renew. Energy Lab. (NREL), Golden, CO, USA, Tech. Rep. NREL/TP-5D00-73476, 2020.

[5] J. Liu, Y. Miura, and T. Ise, "Comparison of dynamic characteristics between virtual synchronous generator and droop control in inverter-based distributed generators," *IEEE Trans. Power Electron.*, vol. 31, no. 5, pp. 3600–3611, May 2016.

[6] J. Song, M. Cheah-Mane, E. Prieto-Araujo, and O. Gomis-Bellmunt, "Short-circuit analysis of AC distribution systems dominated by voltage source converters considering converter limitations," *IEEE Trans. Smart Grid*, vol. 13, no. 5, pp. 3867–3878, Sep. 2022.

[7] W. Wu, Y. Chen, A. Luo, L. Zhou, X. Zhou, L. Yang, Y. Dong, and J. M. Guerrero, "A virtual inertia control strategy for DC microgrids analogized with virtual synchronous machines," *IEEE Trans. Ind. Electron.*, vol. 64, no. 7, pp. 6005–6016, Jul. 2017.

[8] S. D'Arco and J. A. Suul, "Equivalence of virtual synchronous machines and frequency-droops for converter-based MicroGrids," *IEEE Trans. Smart Grid*, vol. 5, no. 1, pp. 394–395, Jan. 2014.

[9] M. Chen, D. Zhou, A. Tayyebi, E. Prieto-Araujo, F. Dörfler, and F. Blaabjerg, "Generalized multivariable grid-forming control design for power converters," *IEEE Trans. Smart Grid*, vol. 13, no. 4, pp. 2873–2885, Jul. 2022.

[10] B. B. Johnson, S. V. Dhople, A. O. Hamadeh, and P. T. Krein, "Synchronization of nonlinear oscillators in an LTI electrical power network," *IEEE Trans. Circuits Syst. I, Reg. Papers*, vol. 61, no. 3, pp. 834–844, Mar. 2014.

[11] M. Lu, "Virtual oscillator grid-forming inverters: State of the art, modeling, and stability," *IEEE Trans. Power Electron.*, vol. 37, no. 10, pp. 11579–11591, Oct. 2022.

[12] *Grid Forming Technology Bulk Power System Reliability Considerations*, NERC, North American Electric Reliability Corporation, Atlanta, GA, USA, 2021.

[13] *AEMO, Voluntary Specification for Grid-Forming Inverters*, Australian Energy Market Operator (AEMO), Melbourne, VIC, Australia, May 2023.

[14] L. Zhang, L. Harnefors, and H.-P. Nee, "Power-synchronization control of grid-connected voltage-source converters," *IEEE Trans. Power Syst.*, vol. 25, no. 2, pp. 809–820, May 2010.

[15] R. Rosso, J. Cassoli, G. Buticchi, S. Engelken, and M. Liserre, "Robust stability analysis of LCL filter based synchronverter under different grid conditions," *IEEE Trans. Power Electron.*, vol. 34, no. 6, pp. 5842–5853, Jun. 2019.

[16] X. Wang, M. G. Taul, H. Wu, Y. Liao, F. Blaabjerg, and L. Harnefors, "Grid-synchronization stability of converter-based resources—An overview," *IEEE Open J. Ind. Appl.*, vol. 1, pp. 115–134, 2020.

[17] T. Qoria, E. Rokrok, A. Bruyere, B. François, and X. Guillaud, "A PLL-free grid-forming control with decoupled functionalities for high-power transmission system applications," *IEEE Access*, vol. 8, pp. 197363–197378, 2020.

[18] Y. Mitsugi and J. Baba, "Phaser-based transfer function analysis of power synchronization control instability for a grid forming inverter in a stiff grid," *IEEE Access*, vol. 11, pp. 42146–42159, 2023.

[19] P. C. Loh and D. G. Holmes, "Analysis of multiloop control strategies for LC/CL/LCL-filtered voltage-source and current-source inverters," *IEEE Trans. Ind. Appl.*, vol. 41, no. 2, pp. 644–654, Apr. 2005.

[20] A. Houari, H. Renaudineau, J.-P. Martin, S. Pierfederici, and F. Meibody-Tabar, "Flatness-based control of three-phase inverter with output *LC* filter," *IEEE Trans. Ind. Electron.*, vol. 59, no. 7, pp. 2890–2897, Jul. 2012.

[21] M. Liserre, F. Blaabjerg, and S. Hansen, "Design and control of an LCL-filter-based three-phase active rectifier," *IEEE Trans. Ind. Appl.*, vol. 41, no. 5, pp. 1281–1291, Oct. 2005.

[22] R. Peña-Alzola, M. Liserre, F. Blaabjerg, R. Sebastián, J. Dannehl, and F. W. Fuchs, "Analysis of the passive damping losses in LCL-filter-based grid converters," *IEEE Trans. Power Electron.*, vol. 28, no. 6, pp. 2642–2646, Jun. 2013.

[23] L. Corradini, P. Mattavelli, M. Corradin, and F. Polo, "Analysis of parallel operation of uninterruptible power supplies loaded through long wiring cables," *IEEE Trans. Power Electron.*, vol. 25, no. 4, pp. 1046–1054, Apr. 2010.

[24] X. Wang, F. Blaabjerg, and W. Wu, "Modeling and analysis of harmonic stability in an AC power-electronics-based power system," *IEEE Trans. Power Electron.*, vol. 29, no. 12, pp. 6421–6432, Dec. 2014.

[25] Q.-C. Zhong, P.-L. Nguyen, Z. Ma, and W. Sheng, "Self-synchronized synchronverters: Inverters without a dedicated synchronization unit," *IEEE Trans. Power Electron.*, vol. 29, no. 2, pp. 617–630, Feb. 2014.

[26] T. Wu, Z. Liu, J. Liu, S. Wang, and Z. You, "A unified virtual power decoupling method for droop-controlled parallel inverters in microgrids," *IEEE Trans. Power Electron.*, vol. 31, no. 8, pp. 5587–5603, Aug. 2016.

[27] H. Wu, X. Ruan, D. Yang, X. Chen, W. Zhao, Z. Lv, and Q.-C. Zhong, "Small-signal modeling and parameters design for virtual synchronous generators," *IEEE Trans. Ind. Electron.*, vol. 63, no. 7, pp. 4292–4303, Jul. 2016.

[28] Z. Shuai, W. Huang, Z. J. Shen, A. Luo, and Z. Tian, "Active power oscillation and suppression techniques between two parallel synchronverters during load fluctuations," *IEEE Trans. Power Electron.*, vol. 35, no. 4, pp. 4127–4142, Apr. 2020.

[29] H. Deng, J. Fang, Y. Qi, Y. Tang, and V. Debusschere, "A generic voltage control for grid-forming converters with improved power loop dynamics," *IEEE Trans. Ind. Electron.*, vol. 70, no. 4, pp. 3933–3943, Apr. 2023.

[30] L. Harnefors, M. Hinkkanen, U. Riaz, F. M. M. Rahman, and L. Zhang, "Robust analytic design of power-synchronization control," *IEEE Trans. Ind. Electron.*, vol. 66, no. 8, pp. 5810–5819, Aug. 2019.

[31] F. Zhao, X. Wang, Z. Zhou, L. Harnefors, J. R. Svensson, L. H. Kocewiak, and M. P. S. Gryning, "Control interaction modeling and analysis of grid-forming battery energy storage system for offshore wind power plant," *IEEE Trans. Power Syst.*, vol. 37, no. 1, pp. 497–507, Jan. 2022.

[32] P. M. Anderson and M. Mirheydar, "A low-order system frequency response model," *IEEE Trans. Power Syst.*, vol. 5, no. 3, pp. 720–729, Aug. 1990.

SOSEUL JEONG (Member, IEEE) received the B.S. and Ph.D. degrees in electrical engineering from Korea University, Seoul, Republic of Korea, in 2017 and 2023, respectively. He is currently a Senior Researcher with Korea Electrotechnology Research Institute. His research interests include power system stability, dynamics and controls of grid-connected converters, HVDC application, and flexible ac transmission systems.

JUNSU PARK (Student Member, IEEE) received the B.S. degree from the Department of Electrical Engineering, Kwangwoon University, Seoul, South Korea, in 2022, where he is currently pursuing the master's degree. His research interests include dynamic analysis of IBRs, impedance modeling of inverters, and power system operation stability.

MINHAN YOON (Member, IEEE) received the B.S. and Ph.D. degrees from the Department of Electrical Engineering, Korea University, Seoul, South Korea, in 2009 and 2015, respectively. He was a Postdoctoral Research Associate with Seoul National University, Seoul, in 2015, and a Senior Engineer with Korea Electrotechnology Research Institute (KERI), from 2015 to 2017. In 2020, he joined the Department of Electrical Engineering, Kwangwoon University, Seoul, as an Associate Professor. His research interests include power system operation and control, including HVDC, FACTS, and IBRs.

○ ○ ○